**Electronic Supplementary Information:**

# MXene with controlled surface termination groups for boosting photoelectrochemical water splitting

Zihao Wu[a,d], Hui Zong[b], Baihe Fu[a], Zhonghai Zhang[a,c,*]

[a] Shanghai Key Laboratory of Green Chemistry and Chemical Processes, School of Chemistry and Molecular Engineer-ing, East China Normal University, Shanghai 200241, China

[b] Key Laboratory of Polar Materials and Devices (MOE), Department of Electronics, East China Normal University, Shanghai 200241, China

[c] Institute of Eco-Chongming, East China Normal University, 20 Cuiniao Road, Chongming District, Shanghai 202162, China

[d] Present address: Beijing National Laboratory for Molecular Sciences College of Chemistry and Molecular Engineer-ing, Peking University, Beijing 100871, China

E-mail: zhzhang@chem.ecnu.edu.cn

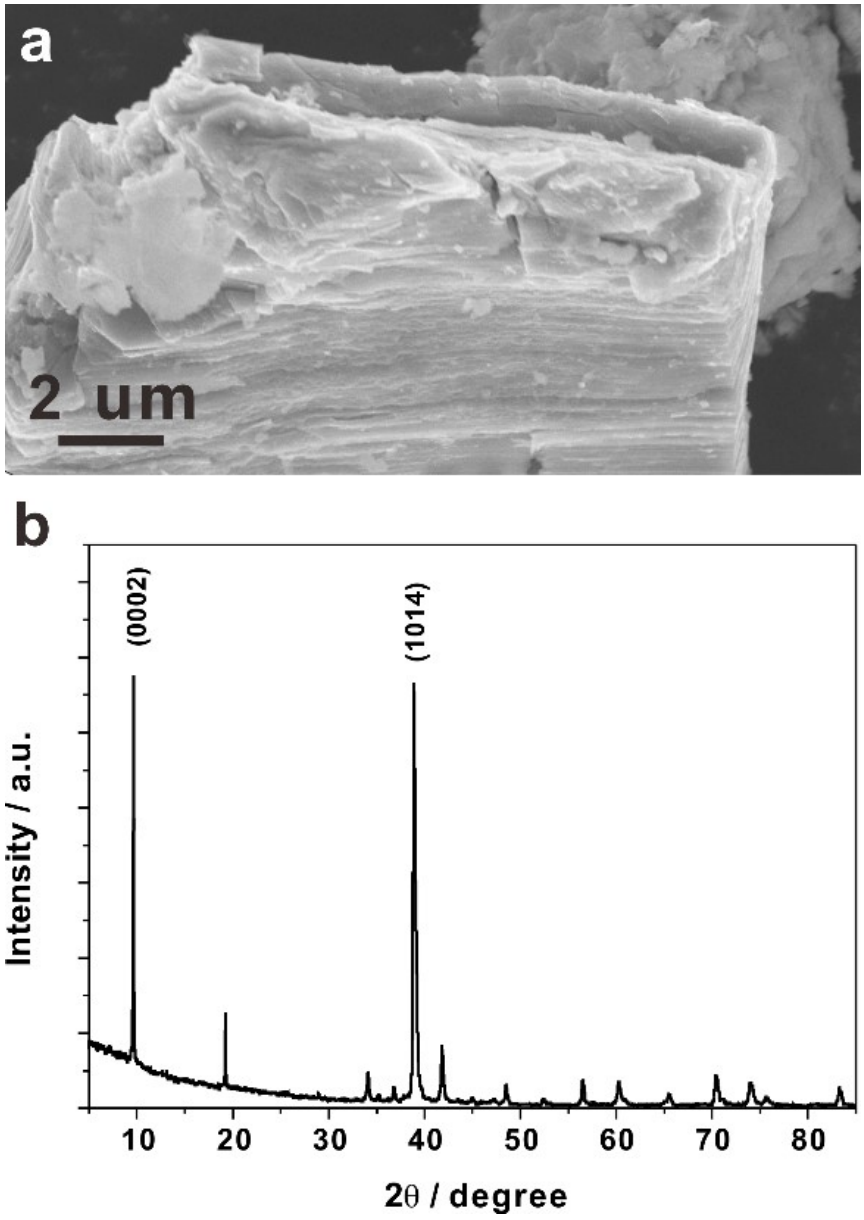


**Fig. S1** SEM image and XRD pattern of MAX phase of $Ti_3AlC_2$.

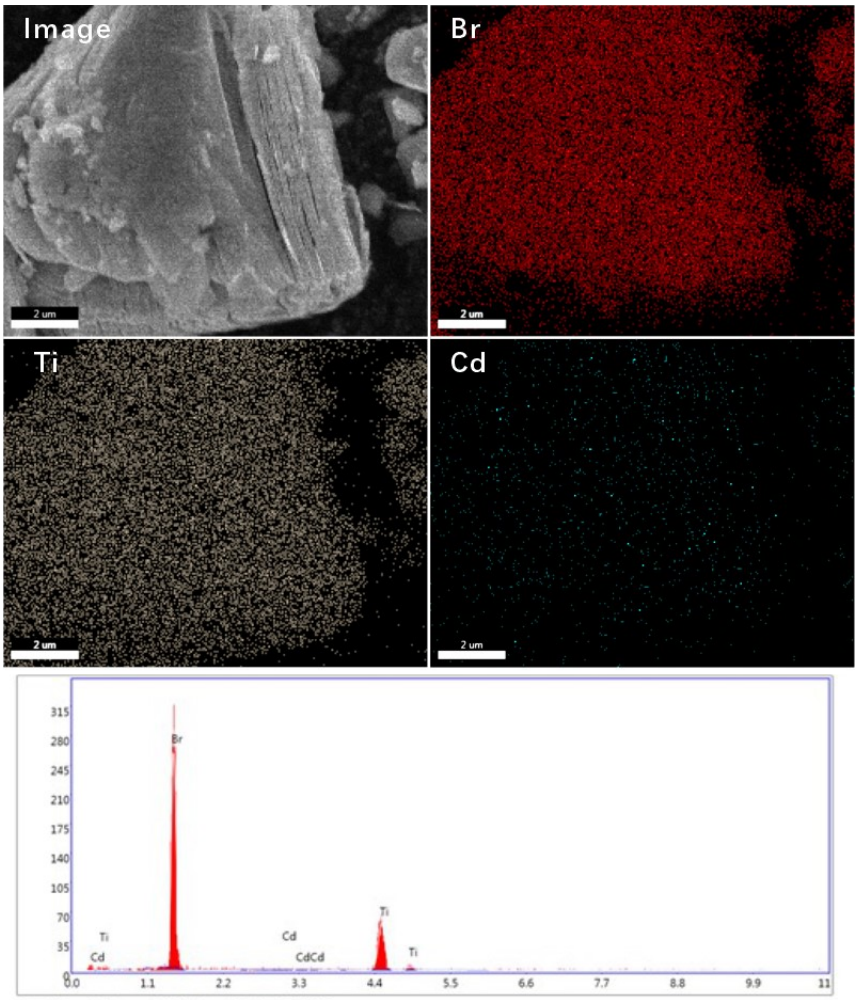


**Fig. S2** SEM image, corresponding elemental mapping, and EDS curve of multilayer Br-MXene.

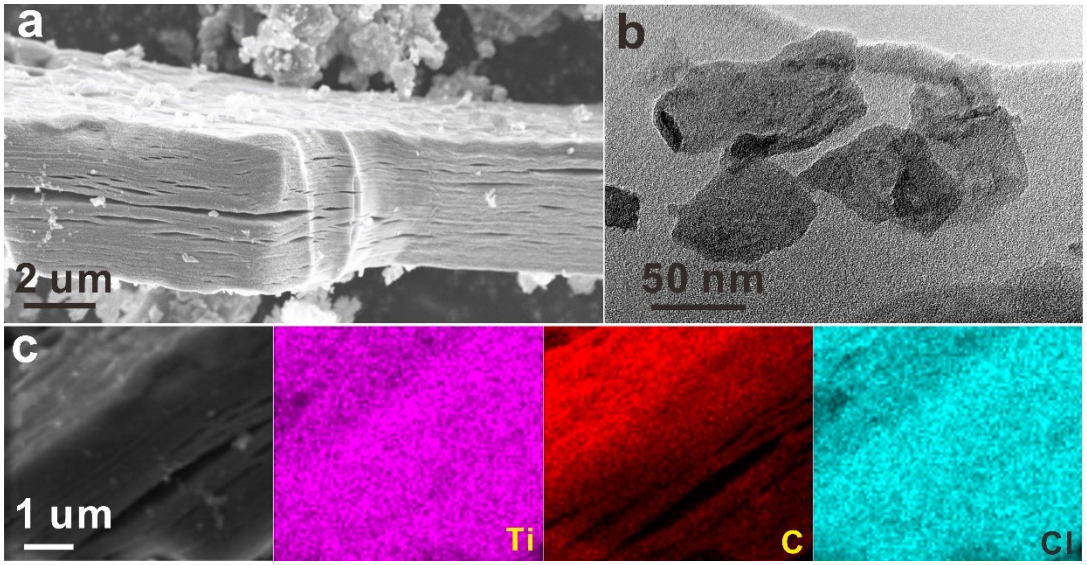


**Fig. S3** Morphology and elemental distribution of Cl-MXene. (a) SEM image of multi-layer Cl-MXene, (b) TEM image of few-layer Cl-MXene, and (c) SEM image and elemental distribution of Ti, C, and Cl of Cl-MXene.

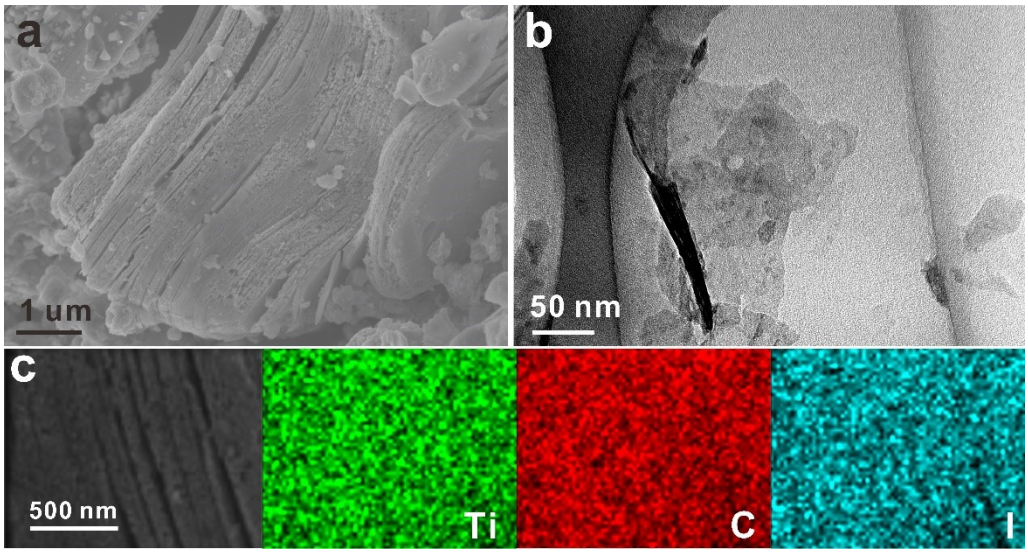


**Fig. S4** Morphology and elemental distribution of I-MXene. (a) SEM image of multi-layer I-MXene, (b) TEM image of few-layer I-MXene, and (c) SEM image and elemental distribution of Ti, C, and I of I-MXene.

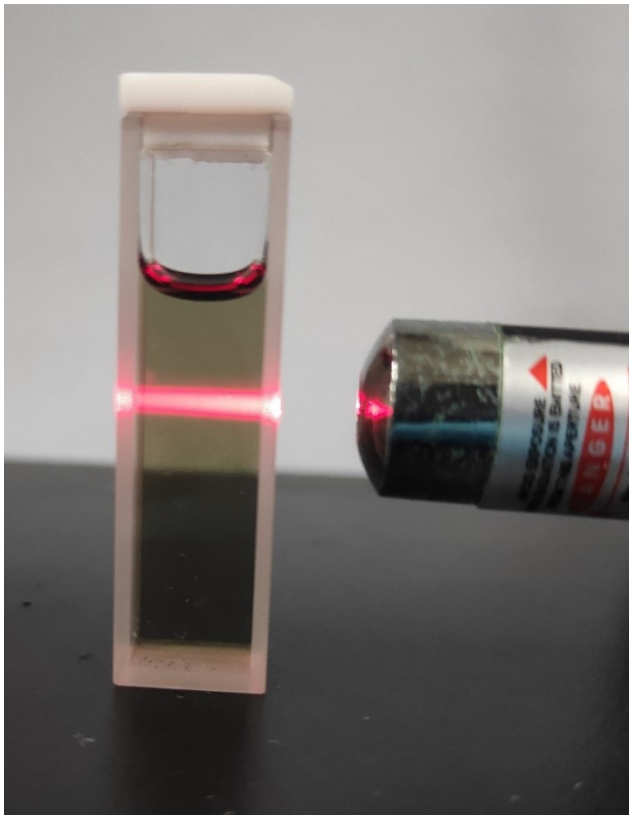

**Fig. S5** Tyndall effect of few-layer Br-MXene in aqueous solution.

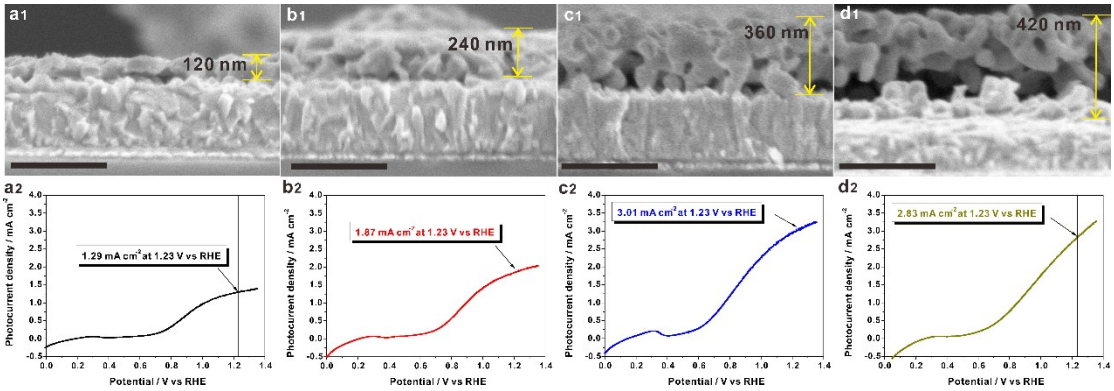


**Fig. S6** Morphological and PEC performance of $BiVO_4$ with different thickness. (a1) Cross-sectional SEM image and (a2) LSV curve under illumination of AM 1.5G of $BiVO_4$ with 120 nm thickness; (b1) cross-sectional SEM image and (b2) LSV curve under illumination of AM 1.5G of $BiVO_4$ with 240 nm thickness; (c1) cross-sectional SEM image and (c2) LSV curve under illumination of AM 1.5G of $BiVO_4$ with 360 nm thickness; (d1) cross-sectional SEM image and (d2) LSV curve under illumination of AM 1.5G of $BiVO_4$ with 420 nm thickness. The scale bar is 500 nm.

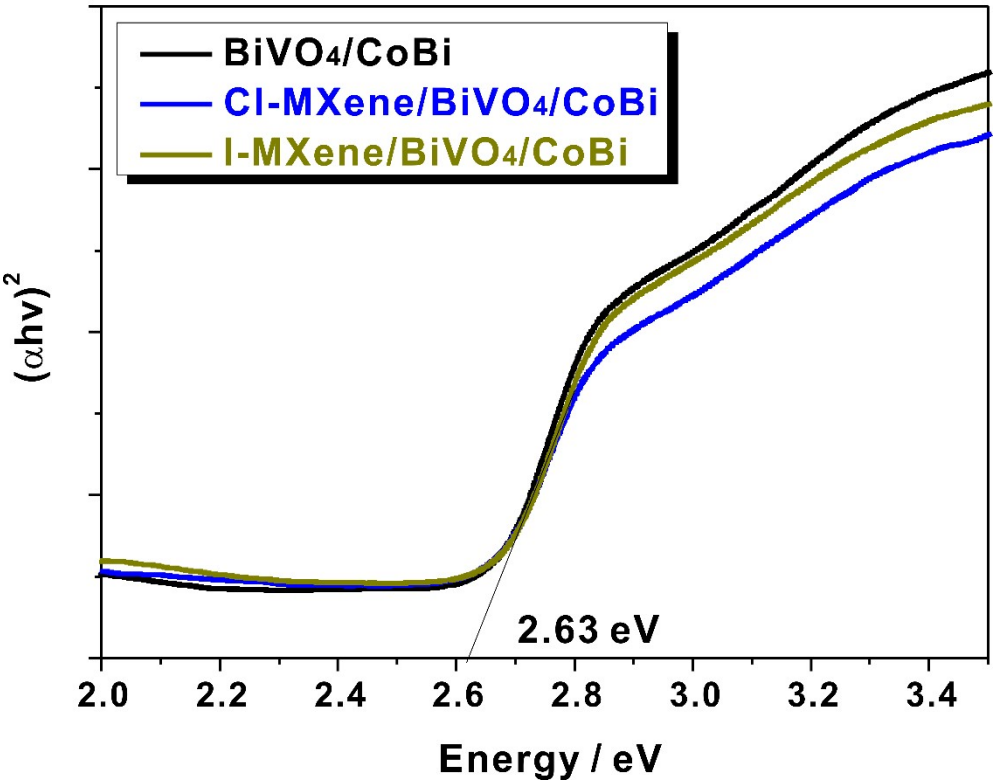


**Fig. S7** Tauc plots of $BiVO_4$/CoBi, Cl-MXene/$BiVO_4$/CoBi, and I-MXene/$BiVO_4$/CoBi.

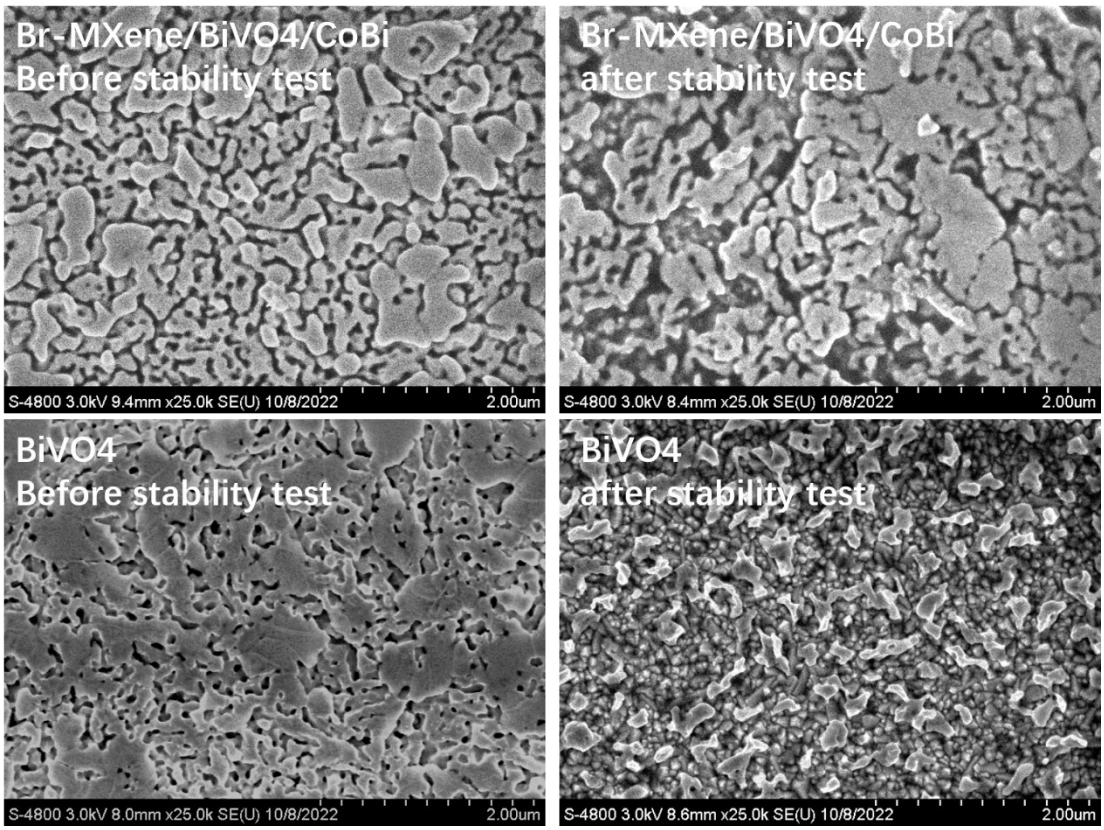


**Fig. S8** SEM image of $BiVO_4$ and Br-MXene/$BiOV_4$/CoBi before and after stability test.

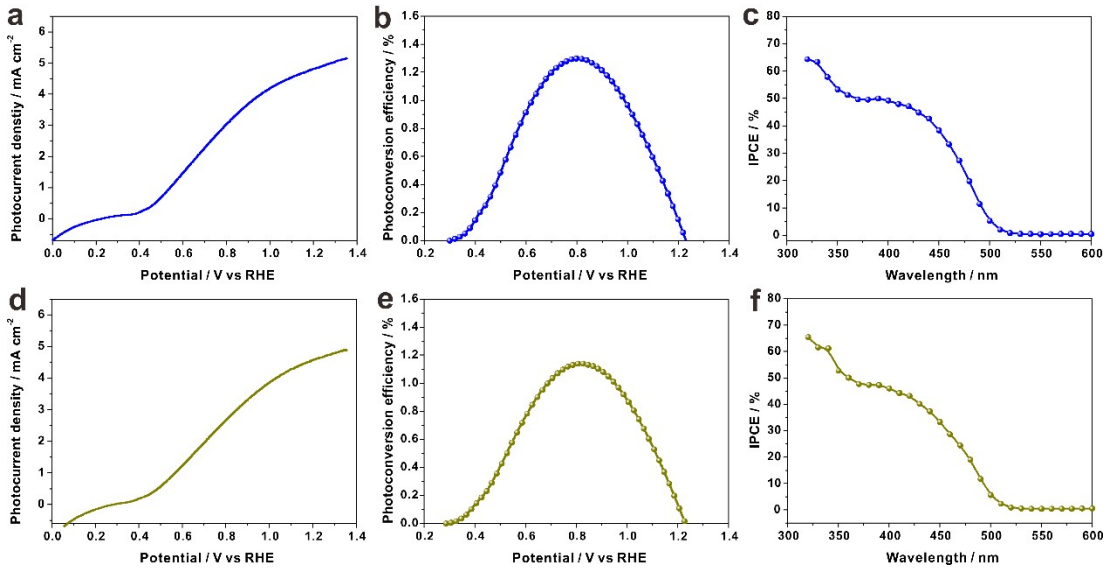


**Fig. S9** PEC performance of Cl-MXene/$BiVO_4$ and I-MXene/$BiVO_4$. (a) LSV curve under illumination of AM 1.5G, (b) photoconversion efficiency at different potentials, and (c) IPCE plot of Cl-MXene/$BiVO_4$/CoBi; (d) LSV curve under illumination of AM 1.5G, (b) photoconversion efficiency at different potentials, and (c) IPCE plot of I-MXene/$BiVO_4$/CoBi.

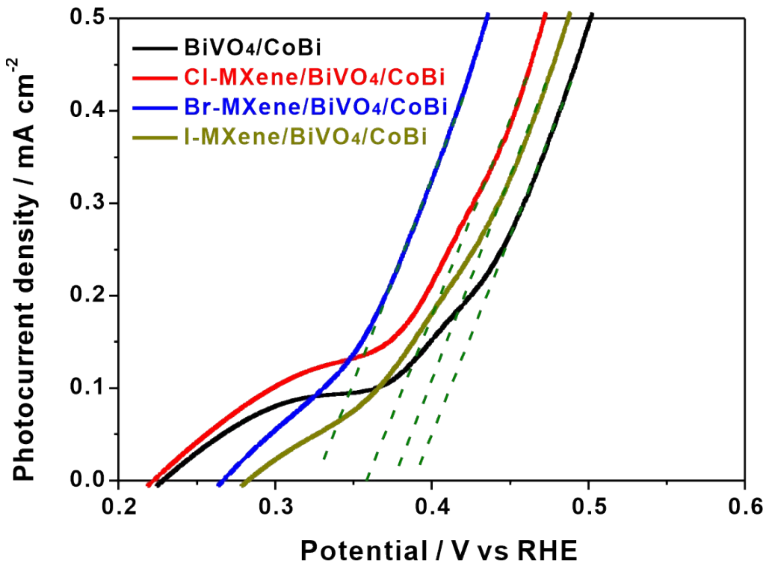


**Fig. S10** Onset potentials of $BiVO_4$/CoBi, Cl-MXene/$BiVO_4$/CoBi, Br-MXene/$BiVO_4$/CoBi, and I-MXene/$BiVO_4$/CoBi photoanodes.

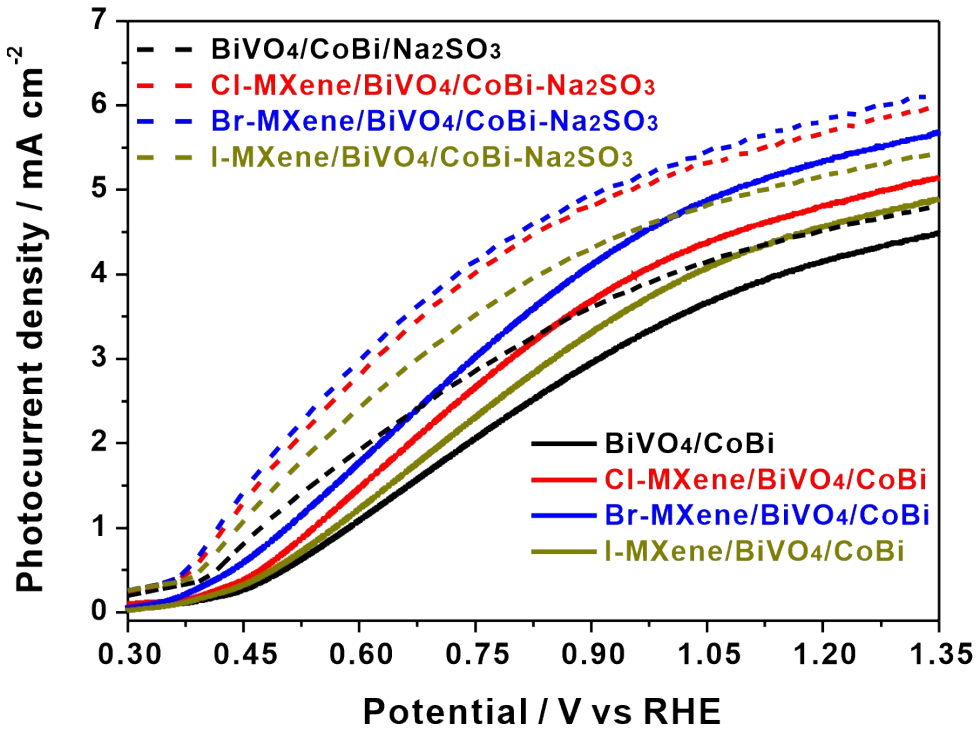


**Fig. S11** LSV curves of $BiVO_4$/CoBi, Cl-MXene/$BiVO_4$/CoBi, Br-MXene/$BiVO_4$/CoBi, and I-MXene/$BiVO_4$/CoBi in the absence and presence of $Na_2SO_3$ under illumination of AM 1.5G.

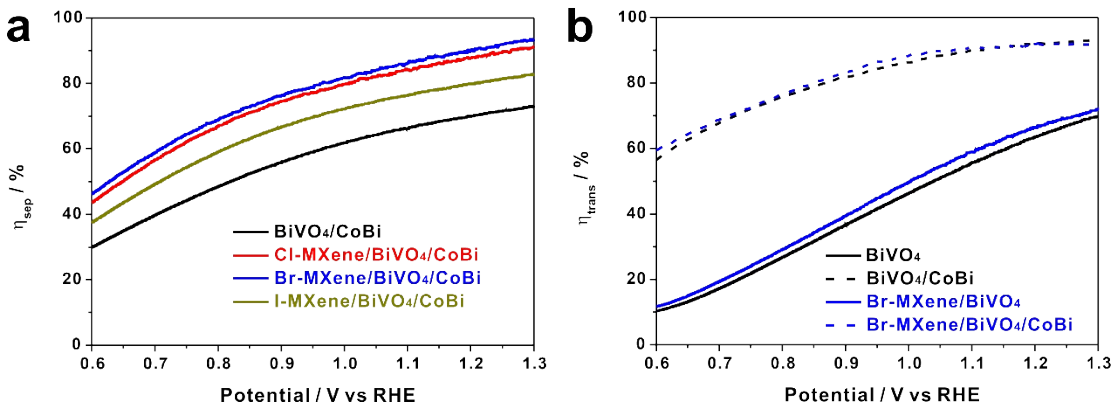


**Fig. S12** (a) Charge separation efficiency on $BiVO_4$/CoBi, Cl-MXene/$BiVO_4$/CoBi, Br-MXene/$BiVO_4$/CoBi, and I-MXene/$BiVO_4$/CoBi; (b) charge transfer efficiency on $BiVO_4$, $BiVO_4$/CoBi, Br-MXene/$BiVO_4$, and Br-MXene/$BiVO_4$/CoBi.

The charge separation efficiency and surface charge transfer efficiency of samples were estimated by using the following equations: [1]

$LHE=1-10^{-A(\lambda)}$

Where $A(\lambda)$ represents absorbance at wavelength equals $\lambda$. The maximum photocurrent density $J_{max}$ was calculated from the number of photons above the photo-active range of $BiVO_4$ under AM 1.5G condition.

$J_{abs} = J_{max} \times LHE$

$\eta_{sep}=J_{Na2SO3}/ J_{abs}$

$\eta_{trans}= J_{water}/ J_{Na2SO3}$

As shown in Fig. S12a, the charge separation efficiency, estimated from comparison of photocurrent density in $Na_2SO_3$ ($J_{Na2SO3}$) and current density expressed from photon absorption rate ($J_{abs}$), on photoanodes of $BiVO_4$/CoBi, Cl-MXene/$BiVO_4$/CoBi, Br-MXene/$BiVO_4$/CoBi, and I-MXene/$BiVO_4$/CoBi were recorded. The Y-MXene/$BiVO_4$/CoBi (Y = Cl, Br, and I) presented certain amount of increase on charge separation efficiency to pristine $BiVO_4$/CoBi, but the increase

was not significant. However, as shown in Fig. S12b, the charge transfer efficiency, estimated from ratios of photocurrent density in water ($J_{water}$) and photocurrent density in $Na_2SO_3$ ($J_{Na2SO3}$), displayed obvious increase after modification of CoBi. The above results helped to indicate the electron transfer layer and hole transfer layer of Y-MXene and CoBi, respectively.

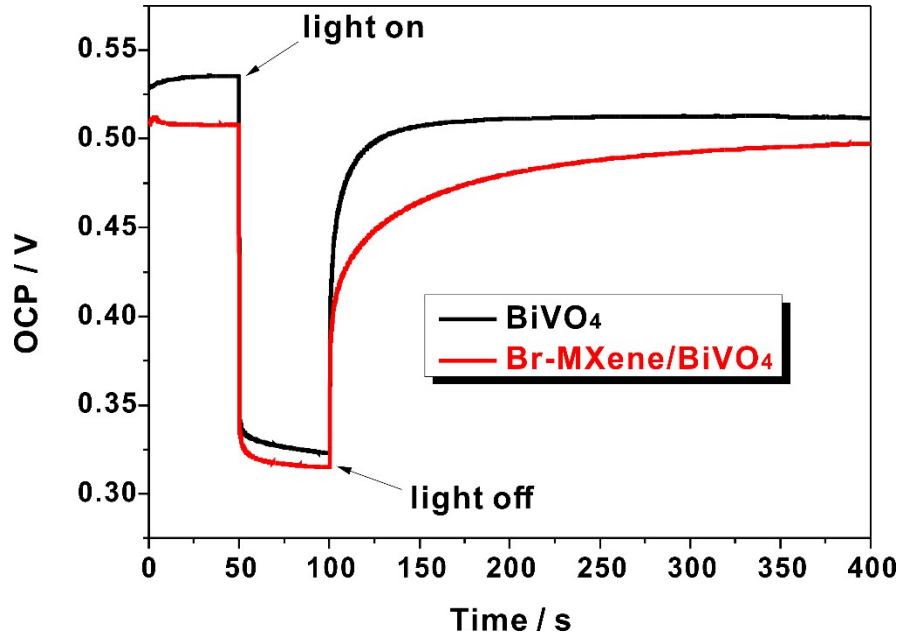


**Fig. S13** Open circuit potential (OCP) of $BiVO_4$ and Br-MXene/$BiVO_4$ with light-on-off model.

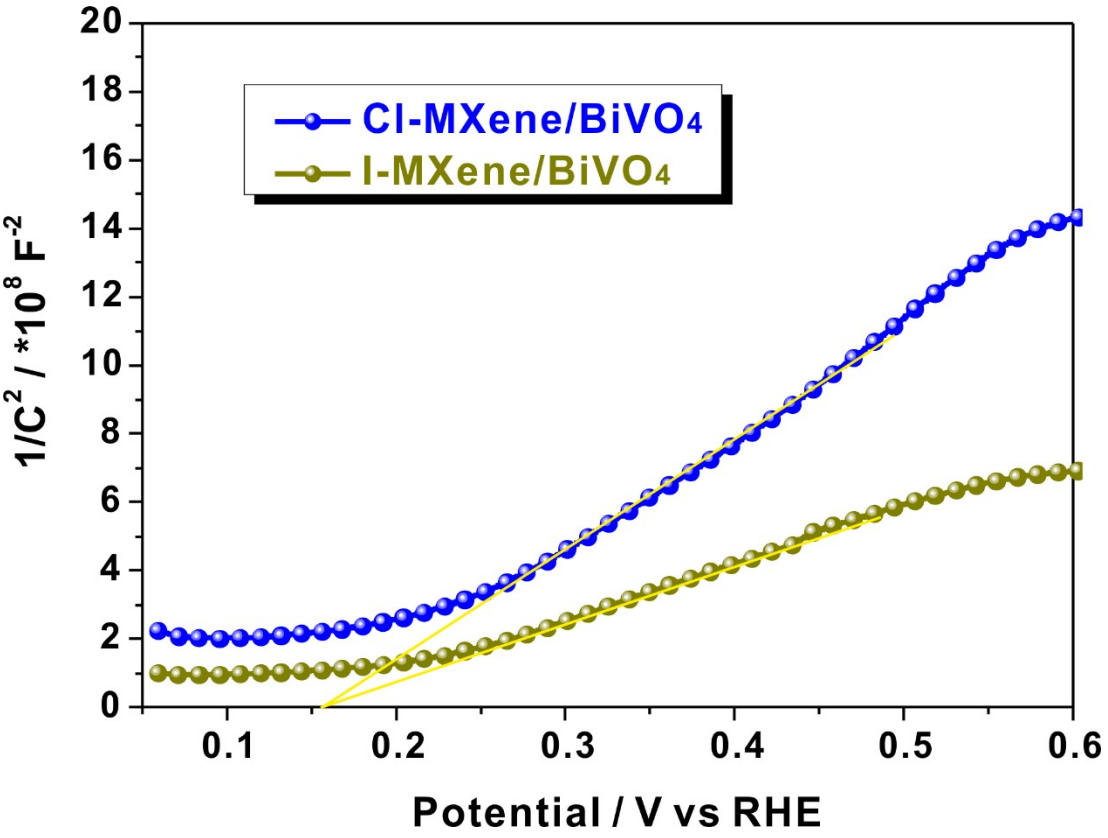


**Fig. S14** Mott-Schottky plots of Cl-MXene/$BiVO_4$ and I-MXene/$BiVO_4$.

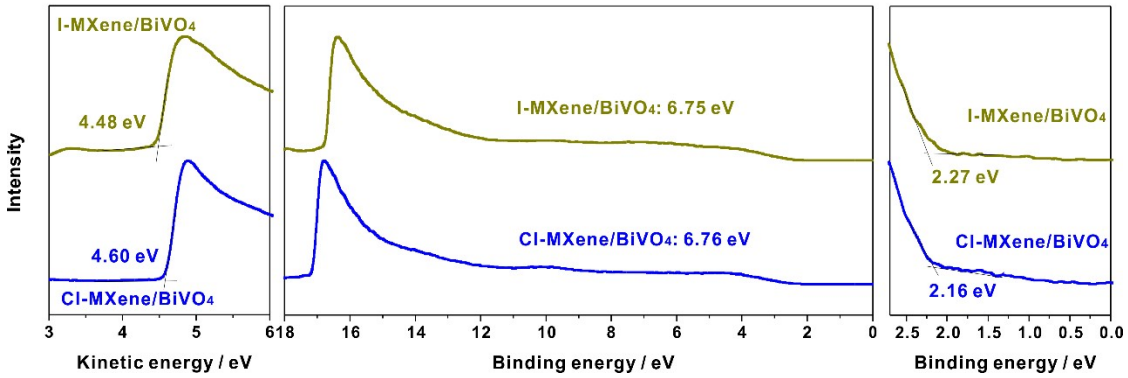


**Fig. S15** UPS and valence spectra of Cl-MXene/$BiVO_4$ and I-MXene/$BiVO_4$.

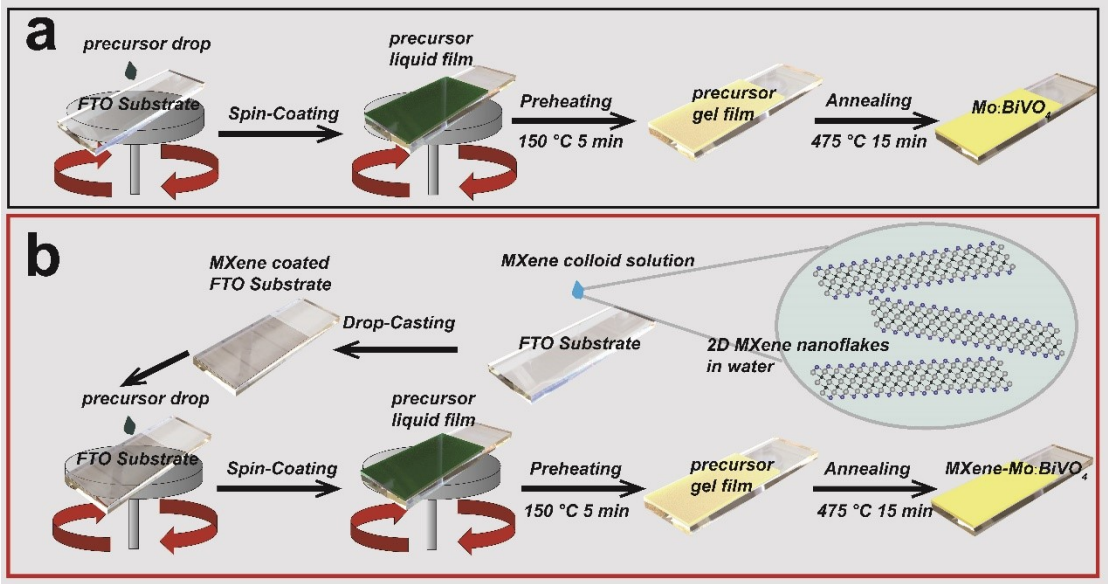


**Fig. S16** Fabrication procedures of (a) $BiVO_4$ and (b) MXene/$BiVO_4$.

**Table S1. Onset potential values on $BiVO_4$/CoBi, Cl-MXene/$BiVO_4$/CoBi, Br-MXene/$BiVO_4$/CoBi, and I-MXene/$BiVO_4$/CoBi photoanodes.**

| Sample | Onset potential (V vs. RHE) |
|---|---|
| $BiVO_4$/CoBi | 0.395 |
| Cl-MXene/$BiVO_4$/CoBi | 0.365 |
| Br-MXene/$BiVO_4$/CoBi | 0.328 |
| I-MXene/$BiVO_4$/CoBi | 0.380 |

**Table S2. Comparison of PEC performance of $BiVO_4$-based photoanodes.**

| Samples | Photocurrent density at 1.23 V vs RHE / mA $cm^{-2}$ | Photocurrent density at 1.23 V vs RHE with hole scavenger / mA $cm^{-2}$ | Stability | Ref |
|---|---|---|---|---|
| Mxene/$BiVO_4$/FeOOH | 4.95 | NA | 77.6% after 2 h | Mater. Today Chem. 2022, 23, 100747 |
| CoNi-MOFs/$BiVO_4$ | 3.2 | NA | 90% after 3 h | Appl. Catal. B, Environ. 2020, 266, 118513 |
| F-$BiVO_4$@NiFe-LDH | 2.67 | NA | Stable for 10 min | Appl. Catal. B, Environ. 2020, 278, 119268 |
| HCoAl-LDH/$BiVO_4$ | 3.5 | NA | 86% after 3 h | Appl. Catal. B, Environ. 2021, 286, 119875 |
| $WO_3$/$BiVO_4$/FeOOH/NiOOH | 5.5 | NA | Stable for 5 h | Nano. Lett. 2017, 17, 8012-8017. |
| R-$BiVO_4$ | 3.18 | 5.84 | NA | ACS Appl. Energy Mater. 2020, 3, 4403-4410 |
| FeCoOx/$BiVO_4$ | 4.82 | 4.82 | Stable for 10 h | Adv. Funct. Mater. 2018, 28, 1802685 |
| Mo:$BiVO_4$/NTO/Fe:NiO | 5.6 | NA | Stable for 16 h | Adv. Funct. Mater. 2021, 31, 2011210 |
| C/$BiVO_4$/CQD | 4.83 | NA | Stable for 9 h | Adv. Funct. Mater. 2022, 32, 2112738 |
| $BiVO_4$/$Fe_xNi_{1-x}OOH$ | 5.8 | NA | Stable for 3 h | Angew. Chem. Int. Ed. 2020, 59, 18990-18995 |
| CoBi/E-$BiVO_4$ | 3.2 | NA | 80% after 1 h | Angew. Chem. 2017, 129, 8620-8624 |
| Ov-$BiVO_4$@NiFe-MOFs | 5.3 | 5.3 | Stable for 10 h | Angew. Chem. Int. Ed. 2021, 60, 1433-1440 |
| FeOOH/rGO/$BiVO_4$ | 3.25 | 4.2 | Stable for 3 h | ChemCatChem 2020, 12, 3769-3775 |
| E-$BiVO_4$/BPQDs/OL-OEC | 6.2 | NA | Stable for 45 h | Energy Environ. Sci. 2022, 15, 672-679 |
| OEC/$MoO_x$/MQD/$BiVO_4$ | 5.85 | NA | 97.5 % after 100 h | Angew. Chem. Int. Ed. 2022, 61, e202200946 |
| NiOOH/BP/$BiVO_4$ | 4.48 | NA | Stable for 60 h | Nat. Commun. 2019, 10, 2001 |
| La:$BaSnO_3$/Mo:$BiVO_4$ | 5.15 | NA | NA | Nat. Commun. 2019, 10, 2609 |
| $NiFeO_x$/B-$C_3N_4$/Mo- | 5.93 | 5.96 | 92% after 10 h | Nat. Commun. 2019, 10, 3687 |

| | | | | |
|---|---|---|---|---|
| $BiVO_4$ | | | | |
| $BiVO_4$/N:$NiFeO_x$ | 6.4 | NA | Stable for 5 h | Nat. Commun. 2021, 12, 6969 |
| nanocone/Mo:$BiVO_4$/Fe(Ni)OOH | 5.82 | 6.05 | 94.2% after 10 h | Sci. Adv. 2016, 2, e1501764 |
| **Br-MXene/$BiVO_4$/CoBi** | **5.47** | **5.91** | **Stable for 20 h** | **This work** |

**Table S3 Flat band potentials and carrier density of $BiVO_4$/CoBi, Cl-MXene/$BiVO_4$/CoBi, Br-MXene/$BiVO_4$/CoBi, and I-MXene/$BiVO_4$/CoBi.**

| Sample | $U_{flat\ band}$ / V vs RHE | ND / $10^{18}$ $cm^{-3}$ |
|---|---|---|
| $BiVO_4$/CoBi | 0.143 | 5.04 |
| Cl-MXene/$BiVO_4$/CoBi | 0.153 | 7.61 |
| Br-MXene/$BiVO_4$/CoBi | 0.187 | 7.54 |
| I-MXene/$BiVO_4$/CoBi | 0.153 | 12.11 |